

A simple method to find temporal overlap between THz and x-ray pulses using x-ray-induced carrier dynamics in semiconductors

Yuya Kubota,^{1, a)} Takeshi Suzuki,² Shigeki Owada,^{3, 1} Kenji Tamasaku,¹ Hitoshi Osawa,³ Tadashi Togashi,^{3, 1} Kozo Okazaki,² and Makina Yabashi^{1, 3}

¹RIKEN SPring-8 Center, 1-1-1 Kouto, Sayo, Hyogo 679-5148, Japan

²Institute for Solid State Physics, The University of Tokyo, Kashiwa, Chiba 277-8581, Japan

³Japan Synchrotron Radiation Research Institute (JASRI), 1-1-1 Kouto, Sayo, Hyogo 679-5198, Japan

(Dated: 7 October 2024)

X-ray-induced carrier dynamics in silicon and gallium arsenide were investigated through intensity variations of transmitted terahertz (THz) pulses in the pico to microsecond time scale with x-ray free-electron laser and synchrotron radiation. We observed a steep reduction in THz transmission with a picosecond scale due to the x-ray-induced carrier generation, followed by a recovery on a nano to microsecond scale caused by the recombination of carriers. The rapid response in the former process is applicable to a direct determination of temporal overlap between THz and x-ray pulses for THz pump-x-ray probe experiments with an accuracy of a few picoseconds.

The development of lasers with ultrashort pulses has revealed transition phenomena to exotic states in condensed matter that cannot be achieved under thermal equilibrium¹. Recently, the technological advancement in the terahertz (THz) frequency range has opened up new horizons in this field². THz light enables resonant excitation in fundamental phenomena, such as the oscillations of lattices and the precessions of spins. Furthermore, THz laser pulses can be used as a driving source of intense electric and/or magnetic fields in the temporal form of mono to a few optical cycles. On the other hand, light with a short wavelength in the x-ray region is very useful as a probe to obtain microscopic properties in electronic and lattice systems. A combination of these distinctive light sources, a THz pump-x-ray probe method, is a powerful technique, which has been used to investigate (super)lattice dynamics after resonant excitations of quasiparticles such as phonon and collective modes of polar vortices³⁻⁵.

Practically, the determination of temporal overlap between THz and x-ray pulses is a technical challenge due to the lack of detectors applicable to both wavelength ranges. For this purpose, near-infrared (NIR) pulses have been frequently used as an intermediary between THz and x-ray pulses. For example, the temporal overlap between the x-ray and NIR laser pulses is determined using reference samples, such as yttrium aluminum garnet (YAG) and bismuth^{6,7}, followed by a determination of the temporal overlap between the THz and NIR laser pulses with the electro-optic (EO) sampling method⁸. However, this method is quite complex. A simple method for determining the temporal overlap with a picosecond accuracy, without using the intermediate NIR pulses, is desirable to efficiently perform the THz pump-X-ray probe experiments.

For this purpose, we investigate the applicability of an x-ray pump-THz probe method. So far, an x-ray pump-NIR probe method helps determine the temporal overlap between x-ray and NIR pulses using the change in transmission of NIR light in materials, such as YAG and gallium arsenide

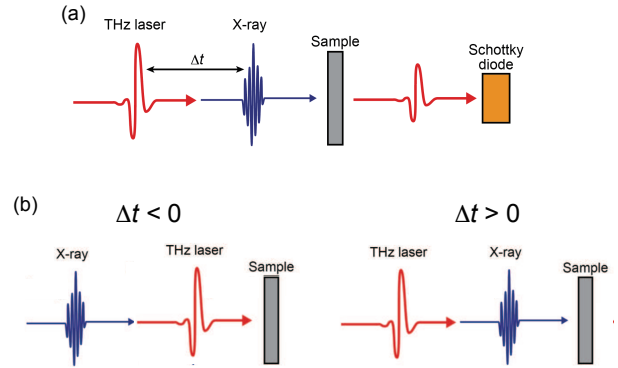


FIG. 1. (a) Schematic of the x-ray pump-THz probe experiment for semiconductors. (b) Schematic of the x-ray and THz pulses reaching the sample. At positive (negative) delay times, the x-ray (THz) reaches the sample first.

(GaAs), excited with intense x-rays^{6,9-11}. X-ray absorption excites electrons, which are then relaxed through secondary processes such as Auger decays and electron-electron scattering. A number of carriers generated in this process changes the sample's refractive index, which is not limited to the NIR region but can be detectable with THz light^{12,13}.

In this study, x-ray pump-THz probe experiments were performed at SPring-8 BL19LXU¹⁴ and SACLA BL3¹⁵. The x-ray-induced carriers in semiconductors were detected with THz pulses, and the temporal response was investigated in the pico to microsecond time scale.

Figure 1(a) shows a schematic drawing of the x-ray pump-THz probe experiment setup. Silicon (Si) wafers with the thickness of 200, 500, and 1000 μm , and a GaAs wafer with the thickness of 700 μm were used as semiconductor samples, which have been extensively studied using an optical pump-THz probe method¹⁶⁻²⁴. The x-ray-induced carrier dynamics were investigated through intensity variations of the transmitted THz pulses detected with a Schottky diode. The signal was amplified and gated with a Boxcar integrator. In this study, a

^{a)}Electronic mail: kubota@spring8.or.jp

delay time (Δt) is defined relative to the x-ray (pump) pulse, as shown in Fig. 1(b).

Figure 2(a) shows a schematic drawing of the THz pulse generation setup using the wavefront-tilted scheme²⁵ at SPring-8 BL19LXU. We used a Ti:sapphire-based regenerative amplifier system with a pulse energy of ~ 0.5 mJ, a pulse duration of 120 fs, a repetition rate of 9 kHz, and a central wavelength of 800 nm. A grating with a groove density of 1200 cm^{-1} was used to tilt the wavefront. The incident angle and diffracted angle of the grating were 4.9 degrees and 60.9 degrees, respectively. The reflected beam was used to detect the THz waveform using the EO sampling method. The image of the grating was transferred to the LiNbO₃ (LN) crystal using L1 and L2 lenses located in the $4f$ configuration. The generated THz pulses were expanded, collimated, and focused using off-axis parabolic (OAP) mirrors. Figures 2(b) and 2(c) show the waveform of the THz pulse evaluated by the EO sampling method with a 300- μm -thick GaP crystal and its Fourier spectrum, respectively.

Figures 2(d) and 2(e) show the time evolution of the differential intensity of transmitted THz pulses between the pumped and unpumped conditions for Si. The samples were excited by x-ray pulses with a repetition rate of 4.5 kHz divided by a chopper. The photon energy $h\nu$, the photon flux, and the size of the x-ray were 10 keV, 5.5×10^6 photons/pulse, and $500 \mu\text{m} \times 500 \mu\text{m}$, respectively. The temporal duration of the x-ray pulse was ~ 40 ps, which dominantly determined the total time resolution. As seen in Figs. 2(d) and 2(e), we observed a rapid decrease in the THz transmission at $\Delta t = 0$, followed by a slow recovery. This behavior suggests the fast generation of electron-hole pairs by the x-ray pulse and the slow recombination of the pairs. These results indicate that the x-ray-induced carriers are detected with THz pulses. The relaxation time of the transmission (τ) was evaluated to be 2.2, 9.2, and 20 μs for Si with the thickness of 200, 500, and 1000 μm , respectively, by fitting using an exponential decay function convoluted with a Gaussian function. These values are comparable to the lifetime of free carriers in Si²⁶.

In contrast to the results on Si, the response of GaAs has distinctive characteristics due to its unique electronic band structure. Figure 3 shows the time evolution of the transmission of THz pulses for GaAs. The relaxation time constant for GaAs is estimated to be 5.6 ns, determined using the same fitting procedure as for Si. This value is significantly shorter than those of Si and agrees with previous reports^{27,28}. This difference is attributed to GaAs having a direct band gap structure, where electrons and holes can recombine efficiently by emitting light. In contrast, Si has an indirect band gap structure, which makes recombination less efficient and results in a longer relaxation time. We will discuss the carrier dynamics in detail later.

To observe the carrier dynamics on the picosecond timescale, we performed an experiment at SACLA BL3 using XFEL pulses with a temporal duration of less than 10 fs²⁹⁻³¹. For SACLA BL3, we adopted a method with two-color laser-induced gas plasma³² to simply generate intense THz pulses, as shown in Fig. 4(a). This is because a shorter pulse duration of 40 fs and higher pulse energy of ~ 12 mJ for the NIR

TABLE I. Plasma frequencies of Si and GaAs, and parameters to evaluate them.

	Si	GaAs
Quantum efficiency Z_0	2.7×10^3	2.4×10^3
Penetration depth d	133.71 μm	51.78 μm
Reduced mass m^*	$0.123m_0$	$0.044m_0$
Plasma frequency f_{pl}	0.73 THz	1.8 THz

laser with a Ti:sapphire-based regenerative amplifier system is available³³. The repetition rate and the central wavelength of the NIR laser were 60 Hz and 800 nm, respectively. A second harmonic pulse at 400 nm was generated with a Beta Barium Borate (BBO) crystal. The fundamental and second harmonic pulses interacted at a focal point of an OAP mirror and generated a THz pulse. The THz pulses were collimated and focused using other OAP mirrors. Figures 4(b) and 4(c) show the waveform of the THz pulse evaluated with the same method as SPring-8 and its Fourier spectrum, respectively.

Figure 4(d) shows the time evolution of the differential intensity of transmitted THz pulses between the pumped and unpumped conditions for Si with a thickness of 500 μm . The photon energy $h\nu$, the pulse energy, the size, and the repetition rate of XFEL were 10 keV, 1.2×10^9 photons/pulse, $344 \mu\text{m} \times 368 \mu\text{m}$, and 30 Hz, respectively. We observed a decrease in the THz transmission due to x-ray-induced carriers, which is consistent with the results obtained at SPring-8. The fall time of the transmission is ~ 20 ps, corresponding to the temporal duration of the THz pulse. Furthermore, we observed an asymmetry shape in the fall of the transmission, where it shows a gradual change in the negative delay range ($\Delta t < 0$) while a steep reduction in the positive delay range ($\Delta t > 0$). This response is explained by the temporal profile of the THz pulse. The THz pulse generated by the gas-plasma method has a main peak at the beginning of the pulse and a long tail, as depicted in Fig. 4(b). In $\Delta t < 0$, the x-ray pulse overlaps with the tail end of the THz pulse, resulting in a gradual change in the THz transmission. In contrast, in $\Delta t > 0$, the x-ray pulse overlaps with the main peak of the THz pulse, and the transmission exhibits a steep change. If we define the beginning of the THz pulse as the time when the intensity changes by more than 3σ from the averaged value in the positive delay range above 20 ps, we were able to determine the temporal overlap with an accuracy of less than 2 ps, as shown in Figs. 4(d). This value is a sufficient accuracy to find the overlap from a wide temporal range in the THz pump-x-ray probe experiments. We note that Fig. 4(e) shows the time evolution of the transmission of THz pulses for GaAs. The response of THz transmission in GaAs shows the same behavior as in Si. This is because the intensity of transmitted THz pulses was reduced to near the detection limit due to the high XFEL pulse energy, and there is no significant difference in the carrier dynamics between the samples in this time scale.

We briefly discuss the difference in the THz transmission between Si and GaAs obtained at SPring-8 BL19LXU. The decrease in the transmission through GaAs is more pronounced than that through Si as shown in Fig. 3. To investi-

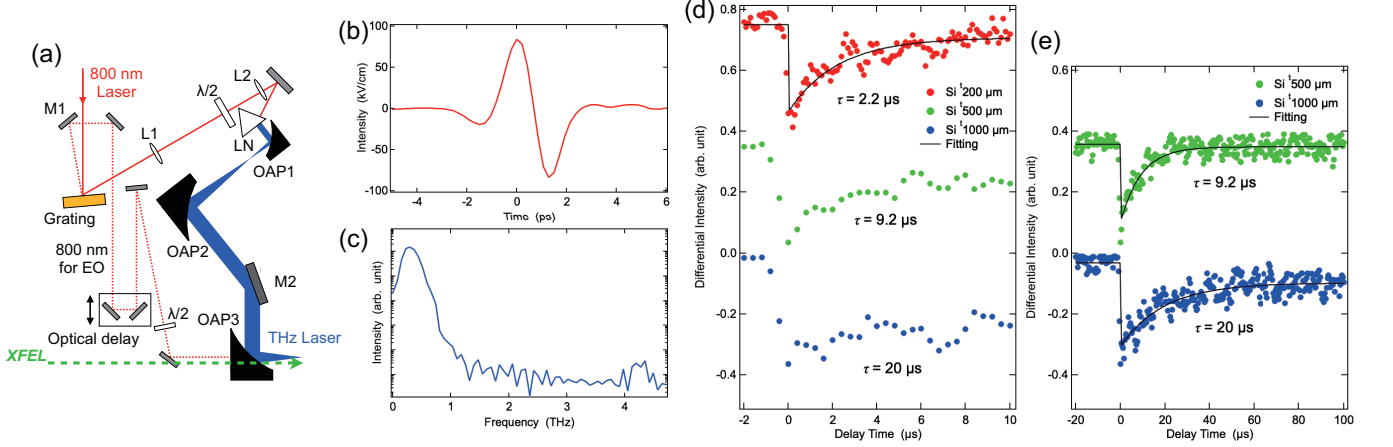


FIG. 2. (a) Schematic of the THz pulse generation setup at SPring-8 BL19LXU. Red solid line: optical path for 800 nm beam, red dashed line: optical path for THz diagnostic, blue bold line: optical path for THz beam. Grating: groove density of 1200 mm^{-1} , L1, L2: lenses, LN: LiNbO₃ crystal, M1: dielectric coated plane mirror, M2: gold-coated plane mirror, OAP: Off-axis parabolic mirror. (b, c) The waveform of the THz pulse evaluated with the EO sampling method (b) and its Fourier spectrum (c). (d, e) Time evolution of the differential intensity of transmitted THz pulses between the pumped and unpumped conditions for Si with the delay range of (d) $[-2 \mu\text{s}, 10 \mu\text{s}]$ and (e) $[-20 \mu\text{s}, 100 \mu\text{s}]$. The red, green, and blue circles represent data for Si with the thickness of 200, 500, and 1000 μm , respectively. The black solid lines represent fitting curves with an exponential decay function convoluted with a Gaussian function.

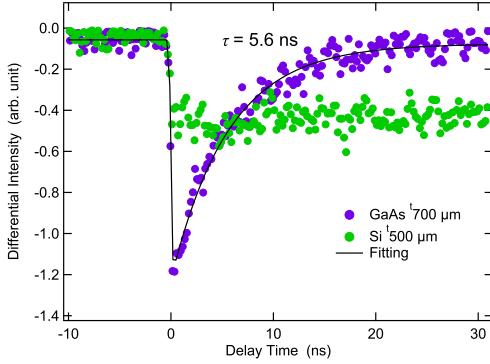


FIG. 3. Time evolution of the differential intensity of transmitted THz pulses between the pumped and unpumped conditions for GaAs with the thickness of 700 μm (purple circles). For comparison, the data for Si with the thickness of 500 μm are also plotted (green circles). The black solid line represents a fitting curve with an exponential decay function convoluted with a Gaussian function.

gate this observation, we performed calculations to determine the plasma frequencies induced by x-ray pulses in both Si and GaAs. Table I summarizes the calculations. Carrier density, N , excited by an x-ray pulse is calculated by

$$N = Z_0 J / xyd, \quad (1)$$

where Z_0 and J are quantum efficiency and photon flux, respectively. We approximate that all x-ray pulse with the size of $x \times y$ is uniformly absorbed within the penetration depth, d . For the x-ray pulse with 10 keV used in this study, the value of Z_0 is 2.7×10^3 (2.4×10^3)³⁴, and d is 133.71 (51.78) μm ³⁵

for Si (GaAs). Using the values of N , the plasma frequency ω_{pl} is calculated by

$$\omega_{\text{pl}} = 2\pi f_{\text{pl}} = \sqrt{\frac{Ne^2}{\epsilon_0 m^*}}, \quad (2)$$

where e and ϵ_0 are electron charge magnitude and permittivity of free space, respectively. The values of the reduced mass of electron-hole (e - h) pairs, $m^* = (1/m_e + 1/m_h)^{-1}$, are $0.123m_0$ for Si³⁶ and $0.044m_0$ for GaAs²⁴, where m_0 is the bare electron mass. The values of f_{pl} are evaluated to be 0.73 THz for Si and 1.8 THz for GaAs in the situation of the experiment at SPring-8 BL19LXU. Because f_{pl} of GaAs is higher than that of Si, GaAs absorbs and reflects the higher frequency components of THz pulses more effectively than Si. This difference leads to a greater reduction in transmission through GaAs than Si. Note that the value of f_{pl} obtained at SACLA BL3 is evaluated to be more than 10 THz for both Si and GaAs. This value indicates that the samples absorb and reflect most of the frequency components of the THz pulses resulting in a large reduction of the transmission.

Figures 2(d) and 2(e) show a sample thickness dependence of the relaxation time in Si. We have also discussed this phenomenon using a simulation with a diffusion equation as shown in the supplementary material.

In summary, the x-ray pump-THz probe experiments for Si and GaAs were performed to establish the simple method to determine the timing overlap between THz and x-ray pulses. The x-ray-induced carrier dynamics were investigated in a wide temporal range from pico to microsecond with XFEL and synchrotron radiation x-ray pulses. The difference in carrier dynamics between Si and GaAs was discussed with their band structures and plasma frequencies. From the presented

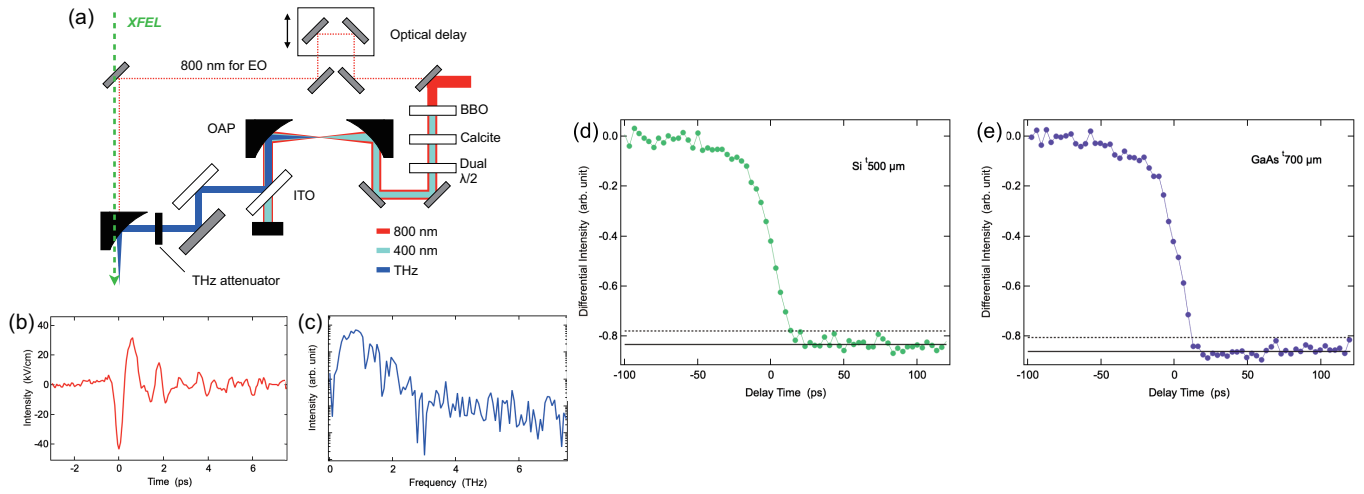


FIG. 4. (a) Schematic of the THz pulse generation setup at SACLA BL3. Red bold line: optical path for 800 nm beam, red dashed line: optical path for THz diagnostic, cyan bold line: optical path for 400 nm beam, blue bold line: optical path for THz beam. BBO: Beta Barium Borate crystal, ITO: indium tin oxide coated mirror, OAP: Off-axis parabolic mirror. (b, c) The waveform of the THz pulse evaluated with the EO sampling method (b) and its Fourier spectrum (c). (d, e) Time evolution of the differential intensity of transmitted THz pulses between the pumped and unpumped conditions for Si with the thickness of $500 \mu\text{m}$ (d) and GaAs with the thickness of $700 \mu\text{m}$ (e). Delay time zero is defined as the center of the falling. Black solid and dashed lines represent the average and 3σ values in the 20 to 170 ps range, respectively.

results, we have confirmed that the method is applicable to the finding of the temporal overlap with an accuracy of a few picoseconds. Due to its simplicity, this method can be adapted to various THz pump-x-ray probe experiments without any changes in the setup.

See the supplementary material for the simulation with a diffusion equation.

This experiment was performed at SPring-8 BL19LXU with the approval of RIKEN (Proposal No. 20210050) and SACLA BL3 with the approval of the Japan Synchrotron Radiation Research Institute (JASRI) (Proposal Nos. 2019B8045 and 2022B8073).

The data that support the findings of this study are available from the corresponding author upon reasonable request.

¹D. N. Basov, R. D. Averitt, and D. Hsieh, *Nat. Mater.* **16**, 1077 (2017).

²T. Kampfrath, K. Tanaka, and K. A. Nelson, *Nat. Photonics* **7**, 680 (2013).

³M. Kozina, T. van Driel, M. Chollet, T. Sato, J. M. Glownia, S. Wandel, M. Radovic, U. Staub, and M. C. Hoffmann, *Struct. Dyn.* **4**, 054301 (2017).

⁴M. Kozina, M. Fechner, P. Marsik, T. van Driel, J. M. Glownia, C. Bernhard, M. Radovic, D. Zhu, S. Bonetti, U. Staub, and M. C. Hoffmann, *Nat. Phys.* **15**, 387 (2019).

⁵Q. Li, V. A. Stoica, M. Paściak, Y. Zhu, Y. Yuan, T. Yang, M. R. McCarter, S. Das, A. K. Yadav, S. Park, C. Dai, H. J. Lee, Y. Ahn, S. D. Marks, S. Yu, C. Kadlec, T. Sato, M. C. Hoffmann, M. Chollet, M. E. Kozina, S. Nelson, D. Zhu, D. A. Walko, A. M. Lindenberg, P. G. Evans, L.-Q. Chen, R. Ramesh, L. W. Martin, V. Gopalan, J. W. Freeland, J. Hlinka, and H. Wen, *Nature* **592**, 376 (2021).

⁶T. Sato, J. M. Glownia, M. R. Ware, M. Chollet, S. Nelson, and D. Zhu, *J. Synchrotron Radiat.* **26**, 647 (2019).

⁷Y. Kubota, Y. Tanaka, T. Togashi, T. Ebisu, K. Tamasaku, H. Osawa, T. Wada, O. Sugino, I. Matsuda, and M. Yabashi, *Appl. Phys. Lett.* **122**, 092201 (2023).

⁸Q. Wu and X. Zhang, *Appl. Phys. Lett.* **67**, 3523 (1995).

⁹M. Harmand, R. Coffee, M. R. Bionta, M. Chollet, D. French, D. Zhu, D. M. Fritz, H. T. Lemke, N. Medvedev, B. Ziaja, S. Toleikis, and M. Cammarata, *Nat. Photonics* **7**, 215 (2013).

¹⁰T. Sato, T. Togashi, K. Ogawa, T. Katayama, Y. Inubushi, K. Tono, and M. Yabashi, *Appl. Phys. Express* **8**, 012702 (2015).

¹¹M. Chollet, R. Alonso-Mori, M. Cammarata, D. Damiani, J. Defever, J. T. Delor, Y. Feng, J. M. Glownia, J. B. Langton, S. Nelson, K. Ramsey, A. Robert, M. Sikorski, S. Song, D. Stefanescu, V. Srinivasan, D. Zhu, H. T. Lemke, and D. M. Fritz, *J. Synchrotron Radiat.* **22**, 503 (2015).

¹²R. Ulbricht, E. Hendry, J. Shan, T. F. Heinz, and M. Bonn, *Rev. Mod. Phys.* **83**, 543 (2011).

¹³E. Zapolnova, R. Pan, T. Golz, M. Sindik, M. Nikolic, M. Temme, M. Rabasovic, D. Grujic, Z. Chen, S. Toleikis, and N. Stojanovic, *J. Synchrotron Radiat.* **27**, 11 (2020).

¹⁴M. Yabashi, T. Mochizuki, H. Yamazaki, S. Goto, H. Ohashi, K. Takeshita, T. Ohata, T. Matsushita, K. Tamasaku, Y. Tanaka, and T. Ishikawa, *Nucl. Instruments Methods Phys. Res. Sect. A* **467-468**, 678 (2001).

¹⁵T. Ishikawa, H. Aoyagi, T. Asaka, Y. Asano, N. Azumi, T. Bizen, H. Ego, K. Fukami, T. Fukui, Y. Furukawa, S. Goto, H. Hanaki, T. Hara, T. Hasegawa, T. Hatsui, A. Higashiya, T. Hirono, N. Hosoda, M. Ishii, T. Inagaki, Y. Inubushi, T. Itoga, Y. Joti, M. Kago, T. Kameshima, H. Kimura, Y. Kirihara, A. Kiyomichi, T. Kobayashi, C. Kondo, T. Kudo, H. Maesaka, X.M. Mar'Al'chal, T. Masuda, S. Matsubara, T. Matsumoto, T. Matsushita, S. Matsui, M. Nagasono, N. Nariyama, H. Ohashi, T. Ohata, T. Ohshima, S. Ono, Y. Otake, C. Saji, T. Sakurai, T. Sato, K. Sawada, T. Seike, K. Shirasawa, T. Sugimoto, S. Suzuki, S. Takahashi, H. Takebe, K. Takeshita, K. Tamasaku, H. Tanaka, R. Tanaka, T. Tanaka, T. Togashi, K. Togawa, A. Tokuhisa, H. Tomizawa, K. Tono, S. Wu, M. Yabashi, M. Yamaga, A. Yamashita, K. Yanagida, C. Zhang, T. Shintake, H. Kitamura, and N. Kumagai, *Nat. Photonics* **6**, 540 (2012).

¹⁶T. Suzuki and R. Shimano, *Phys. Rev. Lett.* **103**, 057401 (2009).

¹⁷T. Suzuki and R. Shimano, *Phys. Rev. B* **83**, 085207 (2011).

¹⁸T. Suzuki and R. Shimano, *Phys. Rev. Lett.* **109**, 046402 (2012).

¹⁹T. Terashige, H. Yada, Y. Matsui, T. Miyamoto, N. Kida, and H. Okamoto, *Phys. Rev. B* **91**, 241201(R) (2015).

²⁰R. Huber, F. Tauser, A. Brodschelm, M. Bichler, G. Abstreiter, and A. Leitnerstorfer, *Nature* **414**, 286 (2001).

²¹R. A. Kaindl, M. A. Carnahan, D. Hägele, R. Lövenich, and D. S. Chemla, *Nature* **423**, 734 (2003).

²²R. Huber, R. A. Kaindl, B. A. Schmid, and D. S. Chemla, *Phys. Rev. B* **72**, 161314(R) (2005).

²³R. A. Kaindl, D. Hägele, M. A. Carnahan, and D. S. Chemla, *Phys. Rev.*

- B 79, 045320 (2009).
- ²⁴F. Sekiguchi, T. Mochizuki, C. Kim, H. Akiyama, L. N. Pfeiffer, K. W. West, and R. Shimano, *Phys. Rev. Lett.* **118**, 067401 (2017).
- ²⁵J. Hebling, G. Alm-Åasi, I. Z. Kozma, and J. Kuhl, *Opt. Express* **10**, 1161 (2002).
- ²⁶D. K. Schroder, *IEEE Trans. Electron Devices* **44**, 160 (1997).
- ²⁷G. W. 't Hooft, W. A. J. A. Van Der Poel, L. W. Molenkamp, and C. T. Foxon, *Phys. Rev. B* **35**, 8281 (1987).
- ²⁸T. Lai, X. Liu, H. Xu, Z. Jiao, J. Wen, and W. Lin, *Appl. Phys. Lett.* **88**, 192106 (2006).
- ²⁹Y. Inubushi, K. Tono, T. Togashi, T. Sato, T. Hatsui, T. Kameshima, K. Togawa, T. Hara, T. Tanaka, H. Tanaka, T. Ishikawa, and M. Yabashi, *Phys. Rev. Lett.* **109**, 144801 (2012).
- ³⁰I. Inoue, K. Tamasaku, T. Osaka, Y. Inubushi, and M. Yabashi, *J. Synchrotron Radiat.* **26**, 2050 (2019).
- ³¹T. Osaka, I. Inoue, J. Yamada, Y. Inubushi, S. Matsumura, Y. Sano, K. Tono, K. Yamauchi, K. Tamasaku, and M. Yabashi, *Phys. Rev. Research* **4**, L012035 (2022).
- ³²D. J. Cook and R. M. Hochstrasser, *Opt. Lett.* **25**, 1210 (2000).
- ³³T. Togashi, S. Owada, Y. Kubota, K. Sueda, T. Katayama, H. Tomizawa, T. Yabuuchi, K. Tono, and M. Yabashi, *Appl. Sci.* **10**, 7934 (2020).
- ³⁴G. Bertuccio and D. Maiocchi, *J. Appl. Phys.* **92**, 1248 (2002).
- ³⁵<https://www.cxro.lbl.gov/>
- ³⁶N. O. Lipari and A. Baldereschi, *Phys. Rev. B* **3**, 2497 (1971).